Draft version March 18, 2019
Preprint typeset using LaTeX style AASTeX6 v. 1.0

# CARBON DETONATION INITIATION IN TURBULENT ELECTRON-DEGENERATE MATTER

Robert Fisher[1,2], Pritom Mozumdar[1], and Gabriel Casabona[1]
[1]Department of Physics, University of Massachusetts Dartmouth, 285 Old Westport Road, North Dartmouth, MA 02740, USA
and
[2]Institute for Theory and Computation, Harvard-Smithsonian Center for Astrophysics, 60 Garden Street, Cambridge, MA 02138, USA

(Dated: March 18, 2019)

## ABSTRACT

Type Ia supernovae (SNe Ia) play a critical role in astrophysics, yet their origin remains mysterious. A crucial physical mechanism in any SN Ia model is the initiation of the detonation front which ultimately unbinds the white dwarf progenitor and leads to the SN Ia. We demonstrate, for the first time, how a carbon detonation may arise in a realistic three-dimensional turbulent electron-degenerate flow, in a new mechanism we refer to as turbulently-driven detonation. Using both analytic estimates and three-dimensional numerical simulations, we show that strong turbulence in the distributed burning regime gives rise to intermittent turbulent dissipation which locally enhances the nuclear burning rate by orders of magnitude above the mean. This turbulent enhancement to the nuclear burning rate leads in turn to supersonic burning and a detonation front. As a result, turbulence plays a key role in preconditioning the carbon-oxygen fuel for a detonation. The turbulently-driven detonation initiation mechanism leads to a wider range of conditions for the onset of carbon detonation than previously thought possible, with important ramifications for SNe Ia models.

*Keywords:* supernovae: general — nuclear reactions, nucleosynthesis, abundances — hydrodynamics — turbulence — white dwarfs

## 1. INTRODUCTION

Type Ia supernovae (SNe Ia) are common luminous transients whose standardizable light curves play a crucial role in cosmology (Phillips 1993). Recent observations of the nearby SN Ia 2011fe and SN 2014J have revealed SNe Ia arise in stellar systems with at least one carbon-oxygen white dwarf (WD) undergoing explosive nuclear burning (Nugent et al. 2011; Churazov et al. 2014). However, no stellar progenitor of a SN Ia event has ever been directly observed, and both their stellar progenitors and the mechanism of the explosion remains a subject of active investigation.

A crucial physical ingredient of SNe Ia is the detonation initiation within the carbon-oxygen WD. A detonation can be initiated in one of two ways: either directly, such as through a shock front, or spontaneously, through a preconditioned mix of heated fuel. Research in the SNe Ia context has focused upon spontaneous initiation, which has been explored by numerous authors, beginning with the work of Blinnikov and Khokhlov (Blinnikov & Khokhlov 1986, 1987). This body of spontaneous initiation work rests upon a theoretical foundation first developed by Zel'dovich and coworkers (Zel'dovich et al. 1970), which invokes a gradient in induction timescales across a region, and which is referred to as the Zel'dovich gradient mechanism.

In this paper, we investigate the role which turbulence plays in preconditioning the thermodynamic state of electron-degenerate matter of WDs under realistic conditions typical of leading SNe Ia channels. We focus upon carbon-oxygen fuel, though the turbulently-driven mechanism we describe relies only upon the fundamental physics of turbulence in an electron-degenerate nuclear reactive medium. Consequently, the basic detonation initiation mechanism is applicable to turbulent regions of mixed carbon, oxygen, and helium electron-degenerate material, which are believed to arise in some SNe I scenarios (Guillochon et al. 2010; Pakmor et al. 2013). We first briefly review the physics of the Zel'dovich gradient mechanism.

## 2. ZEL'DOVICH GRADIENT MECHANISM

In its simplest form, the Zel'dovich gradient mechanism begins with a subsonic laminar deflagration which is initiated at the peak of a temperature gradient. The deflagration proceeds to accelerate into a shock as it propagates down the temperature ramp. Provided that the temperature gradient is sufficiently shallow, the

robert.fisher@umassd.edu

shock does not propagate rapidly in advance of the burning region, and the result is a detonation. In particular, a body of work based upon one-dimensional simulations (Arnett & Livne 1994; Khokhlov et al. 1997; Niemeyer & Woosley 1997; Röpke et al. 2007; Seitenzahl et al. 2009; Holcomb et al. 2013) establishes a critical length scale over which a detonation may be initiated, as a function of background density, temperature, and composition. The Zel'dovich gradient mechanism generally requires a hot background temperature and a shallow temperature gradient on scales that are unresolved in global, full-star 3D SNe Ia simulations, making it challenging to connect the theory to global SNe Ia simulations.

We critically examine the tacit assumption underlying the Zel'dovich gradient mechanism; specifically, that the detonation initiation arises through the development of a laminar flame on a static background. In contrast to this underlying assumption of laminarity, all major SNe Ia channels predict the prevalent hydrodynamic flow conditions to be highly turbulent. For example, in the rapid dynamical phase of a WD merger, the secondary WD is tidally disrupted, and drives turbulence onto the primary through strong shear flows. Turbulent energy is transported from large scales to small scales through the turbulent cascade, dissipating into heat energy, and mixed into deeper layers of the primary WD. For typical accretion velocities on the order of thousands of km/s, the Reynolds number from the accretion flow onto the WD on a characteristic driving length scale of $\sim 100$ km is of order $10^{16}$ (Nandkumar & Pethick 1984). Similar considerations apply to a near-Chandrasekhar mass WD progenitor in the single-degenerate channel, in which the buoyant flame bubble also drives strong, high Reynolds-number turbulence (Niemeyer & Woosley 1997).

We assess the relative importance of nuclear burning and turbulence by computing the ratio of the specific carbon specific nuclear burning rate to the turbulent dissipation rate at densities $\rho \simeq 10^7$ g cm$^{-3}$ at which a detonation is thought likely to arise (Woosley 2007). The mean specific turbulent dissipation rate is $\epsilon_{\rm turb} = 10^{17} \left(v_0/10^3 \text{ km/s}\right)^3 (100 \text{ km}/L)$ erg s$^{-1}$ g$^{-1}$. Here $v_0$ is the RMS turbulent velocity on the integral length scale $L$. Additionally, the specific nuclear burning rate for carbon is highly sensitive to temperature, $\epsilon_{\rm nuc} = 3.65 \times 10^{40} \rho_7^{2.5} X_{12}^2 \exp(-65.894/T_9^{1/3})$ erg s$^{-1}$ g$^{-1}$, including electron screening (Garcia-Senz & Woosley 1995). Here $X_{12}$ is the mass fractional abundance of $^{12}$C, $\rho_7$ is the mass density in units of $10^7$ g cm$^{-3}$, and $T_9$ is the temperature in units of $10^9$ K.

We plot the ratio $\epsilon_{\rm nuc}/\epsilon_{\rm turb}$ versus temperature in figure 1. This plot demonstrates that *heating in carbon-oxygen WD mergers is initially energetically dominated by turbulent dissipation by up to 20 orders of magnitude.* It is also apparent from this figure that an increase of temperature by up to an order of magnitude is required for the fuel in merging carbon-oxygen WDs to enter into the nuclear-dominated regime. The energetics points towards turbulence as playing the dominant role in this process.

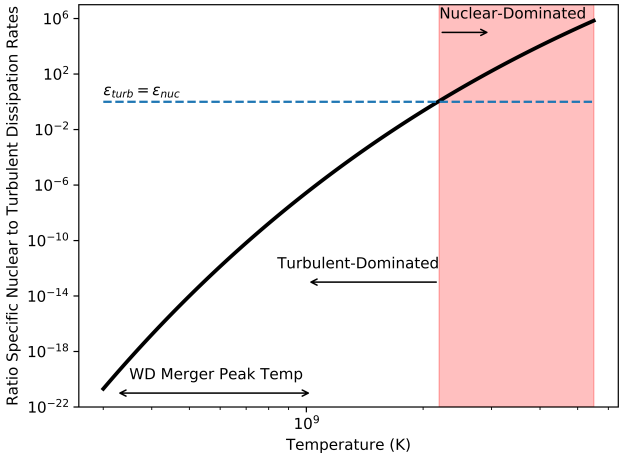


**Figure 1**: Plot of the ratio of the specific nuclear generation rate $\epsilon_{\rm nuc}$ to the specific turbulent dissipation rate $\epsilon_{\rm turb}$, as a function of temperature. The thick solid line shows $\epsilon_{\rm turb}/\epsilon_{\rm nuc}$ as a function of temperature, for the representative values $v_0 = 2 \times 10^3$ km/s, $L = 100$ km, $\rho_7 = 1$, and $X_{12} = 0.5$. The horizontal dashed line demarcates the equality of the specific nuclear burning and turbulent dissipation rates, $\epsilon_{\rm turb} = \epsilon_{\rm nuc}$. The range of peak temperatures achieved in simulations of binary carbon-oxygen WD mergers from Dan et al. (2014) is shown at bottom.

The dominant role of turbulent dissipation has important ramifications for the physical properties of the burning at ignition. At a critical temperature ($T \simeq 7 \times 10^8$ K at $\rho = 10^7$ g cm$^{-3}$), carbon burning overcomes neutrino losses. The relative significance of turbulence upon the burning surface can be quantified by the dimensionless Karlovitz number, Ka $= \sqrt{(u^3/s_l^3) l/L}$, where $u$ is the RMS velocity on the integral scale $L$, and $s_l$ and $l$ are the laminar flame speed and thickness, respectively (Aspden et al. 2008). When Ka $< 1$, turbulence plays a minor role on the scale of the flame, and the flame remains laminar. For large Ka $\gg 1$, the flame is disrupted by the turbulence, and exists in the distributed burning regime. In the distributed burning regime, turbulent mixing strongly dominates the electron conduction, and the products of nuclear burning are isobarically turbulently mixed, with thermal and species diffusion playing negligible roles (Aspden et al. 2008). At densities $\rho \simeq 10^7$ g cm$^{-3}$, the characteristic laminar flame speed is $s_l \sim 4 \times 10^3$ cm/s,

and the flame thickness $l = 4$ cm (Timmes & Woosley 1992). For a typical WD merger driven on length scales $L \simeq 100$ km with RMS turbulent velocity $u = 1-2\times10^3$ km/s, the Karlovitz number Ka $\simeq 10^3 - 10^4$. Consequently, in typical carbon-oxygen WD mergers, nuclear burning is initiated in the distributed burning regime, in strong contrast to the single-degenerate scenario of Chandrasekhar-mass WDs, where nuclear burning is initiated as a flamelet (Niemeyer & Woosley 1997). *Crucially, the central assumption of the Zel'dovich gradient mechanism, namely that detonation initiation arises through the development of a laminar flame on a static background, does not apply to nuclear burning in the highly turbulent distributed burning regime. In particular, the Zel'dovich gradient mechanism omits the dominant role turbulence plays in both heating and transport in this regime.*

Similar criticisms of the Zel'dovich gradient mechanism have been described previously – e.g. Niemeyer (1999). **While the Zel'dovich mechanism is still frequently invoked in the literature, progress has been made towards understanding the nature of turbulent combustion. The challenge of turbulent combustion is at the forefront of combustion research (Poinsot & Veynante 2005). Previous theoretical work in the SN Ia context explored the distributed burning regime using techniques from the combustion literature, including one-dimensional turbulence (Lisewski et al. 2000b; Woosley 2007) and the linear eddy model (Woosley et al. 2009). This work revealed some insights into the nature of the distributed burning regime, in particular that the distributed flame is broadened on the integral scale, and with the turbulent diffusion coefficient acting in place of conduction (Woosley et al. 2009). Later work also developed a subgrid large eddy simulation (LES) model for turbulent nuclear burning (Schmidt et al. 2006) and incorporated an analytic deflagration-to-detonation model based upon turbulently intermittent velocity fluctuations (Schmidt et al. 2010; Ciaraldi-Schoolmann et al. 2013).**

**Three-dimensional direct numerical simulations (DNS) of the microphysical evolution of turbulent flames on the flame scale in the context of terrestrial combustion have revealed that for sufficiently strong turbulence, the flame structures become packed together and collide, and lead to enhanced burning and detonation initiation (Poludnenko et al. 2011; Poludnenko 2015). These simulations have only been conducted in non-degenerate gases undergoing chemical combustion. However, the basic physical mechanism, a generalization of the Richtmyer-Meshkov instability in a reactive medium (Poludnenko 2015), shows promise in potentially explaining the deflagration-to-detonation transition (DDT) in near-$M_{\rm Ch}$ WDs in the SD channel. In particular, in a near $M_{\rm Ch}$ WD, burning is initiated in the flamelet regime, and moves into the distributed burning regime as the flame moves to lower densities, becoming subject to the instability described by Poludnenko (2015), and possibly undergoing a DDT.**

**In contrast, in this paper, we focus upon burning which is initiated at low densities $\sim 10^7$ g/cm$^3$ in the distributed burning regime, such as is thought to arise in the double degenerate channel of merging white dwarfs. In this regime, the burning is distributed over the integral scale, and as a consequence, we focus our investigation on these larger scales. The possible importance of turbulent dissipation in initiating a detonation front in the distributed burning regime was first suggested by Woosley (2007). Pioneering 3D simulations of the distributed burning regime have been subsequently carried out by Aspden et al. (2008) and Fenn & Plewa (2017).** However, to date, no multidimensional SN Ia simulation in the literature has been carried into the detonation phase, motivating the current investigation. We proceed to describe the physics of the turbulently-driven detonation mechanism.

## 3. TURBULENTLY-DRIVEN DETONATION MECHANISM

In the turbulently-driven detonation mechanism, carbon-rich electron-degenerate fuel is heated by strong turbulent dissipation, initiating the formation of a hot spot, and subsequently leading to supersonic burning and a detonation. The pressure support of the fuel is primarily derived from electron degeneracy, and as a result, the fuel does not rapidly respond to the turbulent heating. Turbulent dissipation is intrinsically highly intermittent, and is distributed inhomogeneously throughout the burning volume (Kolmogorov 1962; Oboukhov 1962). In particular, in subsonic turbulence, the turbulent cascade is locally dissipated in highly-intermittent vortical structures, consistent with a log-Poisson statistical distribution of turbulent dissipation (She & Leveque 1994; Dubrulle 1994). This intermittent dissipation gives rise to an intermittent temperature distribution on small scales, and naturally preconditions the carbon-rich fuel for a detonation. Furthermore, while the fuel must be at sufficiently low density to be in the distributed burning regime, turbulence suffices to both precondition and ignite the fuel. A strong pre-existing deflagration

front is therefore not a prerequisite to achieve a detonation, as in previous deflagration-to-detonation transition (DDT) models (Khokhlov et al. 1997).

Hot spots arise from local temperature maxima in the turbulent flow. These hots spots have a nuclear burning timescale $\tau_{\rm nuc} = e_{\rm int}/\epsilon_{\rm nuc}$ required to increase the specific internal energy $e_{\rm int}$. Additionally, each turbulent hot spot of size $r$ is associated with an eddy turnover time, $\tau_{\rm edd} = r/v_r$, where $v_r$ is the Kolmogorov turbulent RMS velocity on the length scale $r$, $v(r) = v_0\,(r/L)^{1/3}$.

Because carbon burning is dominated by turbulent dissipation in the distributed burning regime, in most local temperature maxima, the eddy turnover time is shorter than the nuclear burning timescale. Under these conditions, the hot spot will turbulently mix into the surrounding cooler material, and dissipate more rapidly than nuclear burning can increase its temperature. However, for temperature fluctuations at the upper tail of the temperature distribution, the eddy turnover time may be longer than the nuclear burning timescale, at which point the eddy will undergo a nuclear runaway (Lisewski et al. 2000b). One-dimensional models of distributed burning estimate a critical minimum scale of order $\simeq 1$ km for the onset of supersonic burning and detonation initiation (Woosley 2007). For scales $r \simeq 1$ km, and for typical turbulent driving parameters $v_0 = 2 \times 10^3$ km/s and $L = 100$ km, the nuclear burning timescale falls beneath the eddy turnover time $\tau_{\rm nuc} < \tau_{\rm edd}$ at a critical temperature $T_{\rm crit} \simeq 2 \times 10^9$ K. Moreover, because of the temperature sensitivity of the carbon nuclear burning rate, a large change in any of the turbulent driving parameters results in only a small change in the critical temperature $T_{\rm crit}$, which is generally expected to closely correspond to the transition into the nuclear-heating dominated regime.

## 4. SIMULATION METHODOLOGY

In order to understand the physics of the turbulently-driven detonation initiation mechanism, we have carried out 3D simulations. We employ the FLASH hydrodynamics code, and utilize the split piecewise parabolic method (PPM) hydrodynamics solver. We use an equation of state which includes contributions from nuclei, electrons, and blackbody photons, and which supports an arbitrary degree of degeneracy and special relativity for the electronic contribution (Timmes & Swesty 2000). Nuclear burning is incorporated using a 19-isotope network with 78 rates described by Weaver et al. (1978), and optimized in a hard-wired implementation detailed by Timmes (1999).

The fully-periodic domain is chosen to have size $L = 100$ km, with an initially uniform mass density $10^7$ g cm$^{-3}$, temperature $10^8$ K, and zero velocity. The initial composition is assumed to be equal proportions of carbon and oxygen. The momentum of the simulation is then driven to a steady state using a large-scale stochastic forcing routine which has been extensively verified against other numerical simulations, and validated against experiments (Benzi et al. 2008; Arnèodo et al. 2008; Benzi et al. 2010). The stirring is done over waveumbers 1 - 4 with a smooth paraboloidal injection of power, a solenoidal weight $\xi = 0.5$ providing roughly equal power in compressible and incompressible modes, and an autocorrelation time of 0.05 s (Federrath et al. 2010). Nuclear burning is turned on once the model achieves steady-state turbulent velocity statistics, establishing the zero point of our simulation clock, $t = 0.0$, at which point the models had mean temperatures $T_{\rm mean} \simeq 10^9$ K. Four simulations were conducted, with spatial resolutions varying of $64^3$, $128^3$, $256^3$, and $512^3$. Each simulation had identical turbulent driving strengths, achieving 3D RMS velocities $v_{\rm rms} = 2.2 \times 10^3$ km/s in steady-state, with the highest resolution simulations having 3% higher turbulent RMS velocities than our lowest-resolution model. Under these conditions, the mean Karlovitz number Ka $= 8 \times 10^3$, and nuclear burning is accurately treated in a fully distributed fashion without incorporating electron conduction or a flame model.

| Resolution | $T_{\rm mean}$ (K) | $t_{\rm det}$ (ms) |
|---|---|---|
| $64^3$ | $1.12 \times 10^9$ | 12 |
| $128^3$ | $1.17 \times 10^9$ | 14 |
| $256^3$ | $1.17 \times 10^9$ | 13 |
| $512^3$ | $1.18 \times 10^9$ | 15 |

**Table 1**: A summary of key results for the runs in this paper, including the mass-weighted mean temperature and time at detonation.

## 5. SIMULATION RESULTS

### 5.1. *Turbulence Verification and Validation*

**As described, the stochastically-driven turbulence methodology employed here (Federrath et al. 2010) is built upon an earlier implementation which has been rigorously verified against simulation data and validated against experiment, for both Eulerian and Lagrangian properties, in an extensive series of papers (Fisher et al. 2008; Benzi et al. 2008; Arnèodo et al. 2008; Benzi et al. 2010). Here, we reproduce key results to confirm the expected statistical properties of the turbulence, prior to the initiation of nuclear burning.**

**In particular, for the purposes of verification and validation, we focus upon the properties of the velocity structure functions. The $p$th-**

order longitudinal structure function is defined as the volume-averaged moment of the velocity increment probability distribution function. In the $x$ direction, the longitudinal velocity structure function is $\langle |v_x(x+r) - v_x(x)|^p \rangle \propto r^{\zeta_p}$, where the brackets indicate averaging over space and the proportionality applies in the inertial range. Here $\zeta_p$ is the $p$th order longitudinal velocity structure function scaling exponent. As a consequence of Kolmogorov's first similarity hypothesis, which assumes that small-scale turbulence restores the homogeneous and isotropic symmetries broken by the large-scale flow, Kolmogorov's 1941 theory predicts that $\zeta_p = p/3$ (Frisch 1995). Extensive experiments and numerical simulations have conclusively demonstrated that the existence of small-scale inhomogeneity and anisotropy stemming from intermittent dissipation causes the longitudinal velocity structure function scaling exponents to deviate from Kolmogorov's original prediction. Because of the deviation from the 1941 theory prediction, these scalings are frequently referred to as "anomalous."

We have measured the anomalous longitudinal velocity structure function exponents for our $512^3$ model for each of the three cardinal directions using the extended self-similarity technique, which substitutes the third-order structure function for the coordinate $r$. By an exact relation, Kolmogorov's $4/5$th law, the third-order structure function is proportional to $r$ in the inertial regime. Extended self-similarity exploits the $4/5$th law to obtain improved scaling relations for the other structure functions, thereby allowing more accurate and precise measurements of the anomalous scaling exponents (Benzi et al. 1993). The three scaling exponents obtained at the end of the driving phase for our $512^3$ run are, in the three cardinal directions, $\zeta_{2,x} = 0.688$, $\zeta_{2,y} = 0.689$, and $\zeta_{2,z} = 0.686$. The exponents obtained in each of the three directions agree to better than 0.5%, indicating a high degree of spatial isotropy in the velocity field.

Furthermore, the measured anomalous scaling exponents are in excellent agreement within one standard deviation of recent experimental measurements in a closed rotating flow, made with extended self-similarity ($0.69 \pm 0.005$), or globally ($0.68 \pm 0.03$) (Saw et al. 2018), and with numerical simulation ($0.701 \pm 0.014$) (Gotoh et al. 2002), and within 1% of theory (0.696) (She & Leveque 1994). The measured second-order scaling exponents are also within one standard deviation of our own previously-published result $0.71 \pm 0.02$ (Benzi et al. 2010) obtained at higher resolution ($1856^3$) and effective Reynolds number, demonstrating the reproducability of our methodology.

The longitudinal velocity structure function can also be related to the kinetic energy power spectrum through well-known identities (Pope 2000). In particular, the one-dimensional turbulent kinetic energy power spectrum index inferred from the mean of the three cardinal directions is $-(1+\zeta_3) = -1.69$, close to the canonical value of $-5/3 = -1.67$, but including the intermittency corrections due to anomalous scaling. Similarly, the dimensionless prefactor in the second-order structure function is related to the dimensionless prefactor in the turbulent kinetic energy power spectrum, a value also known as Kolmogorov's constant. We infer a Kolmogorov constant of 0.42, which is within two standard deviations of the average over many experiments $0.53 \pm 0.055$ at higher effective Reynolds numbers (Sreenivasan 1995). The lower value inferred from our dataset is consistent with the observed trend of lower Kolmogorov constants at lower effective Reynolds numbers (Sreenivasan 1995).

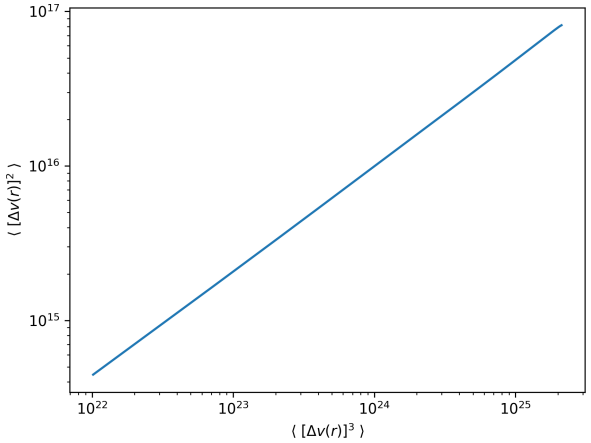


**Figure 2**: A plot of the second-order longitudinal velocity structure function versus the third-order longitudinal velocity structure function. The scaling of this plot accurately yields the second-order velocity structure function scaling exponent $\zeta_2$ by the extended self-similarity technique.

### 5.2. *Nuclear Burning and Detonation Initiation*

We examine the results of 3D numerical simulations of strongly-driven turbulent distributed nuclear burning. We first examine the spatial distribution of temperature

and nuclear burning. In figure 3, we show slice plots in the $y$-$z$ plane of both temperature and log specific nuclear burning rate for the highest-resolution $512^3$ run. These slices are centered about the maximum temperature, and taken a time just prior to the onset of rapid nuclear burning and detonation initiation. Because of the temperature sensitivity of the carbon burning rate, the burning rate is strongly correlated with the temperature distribution. The insets in figure 3 show the resolved hot spot, of order a few km in extent, which develops into a detonation.

Turbulent fluctuations in the dissipation rate give rise to a statistical distribution of temperatures and also of nuclear burning rates. We quantify this temperature distribution in the one-point probability distribution functions (PDFs) of temperature and specific nuclear burning rates, shown in figure 5, for each of our four runs. **Because of the extreme sensitivity of the carbon nuclear burning rate to temperature, care was taken to plot each of the PDFs at the same maximum temperature, $2\times10^9$ K.** The temperature PDF is approximately Gaussian, in agreement with experiments of grid-generated wind tunnel turbulence, which find Gaussian temperature PDFs in the absence of mean temperature gradients (Jayesh & Warhaft 1991).

Additionally, we quantify the turbulent enhancement of the carbon burning rate in figure 5, where we plot the PDF of the specific carbon burning rate, normalized to the mean rate, for all runs. Because the carbon burning rate is highly sensitive to temperature, the relatively modest fluctuations in the temperature result in enhancements in the carbon burning rate by four orders of magnitude above the mean.

A key question is to what extent the simulation results depend upon the spatial resolution; that is, whether the simulations are spatially and temporally converged. At the lower resolution models of $64^3$ and $128^3$, the temperature PDF exhibits extended tails in comparison to those at higher resolutions. The resulting simulations detonate at slightly earlier times and lower mean temperatures than higher-resolution models. In contrast, the models at $256^3$ and $512^3$ demonstrate a high degree of convergence. In particular, the mean temperature at the time of detonation is converged to within 1% at the highest resolution.

In figure 4, we show the time-evolution of the ratio of the eddy-turnover time $t_{\rm edd}$, to the burning timescale $t_{\rm burn} = X(^{12}{\rm C}) \,/\, \dot{X}(^{12}{\rm C})$ at the temperature maximum, as well as the minimum $^{12}$C abundance at the location of the temperature maximum for the $512^3$ model. **Here we have taken the eddy-turnover time on the length scale $r = 1$ km, estimated earlier as the critical length scale for ignition under these conditions.** Initially, this ratio $t_{\rm edd}/t_{\rm burn}$ in the 3D simulation is already orders of magnitude larger than that predicted by the mean temperatures in the absence of turbulence as shown in figure 3, because of the enhancement in the nuclear burning rate due to intermittent temperature fluctuations. The ratio $t_{\rm edd}/t_{\rm burn}$ is still initially less than unity, meaning that the nuclear burning is initially stable. As the simulation evolves, the ratio increases periodically as hot spots develop and are turbulently mixed into the background. At $t = 0.015$ s, or approximately three global eddy turnover times, a hot spot develops in which nuclear burning develops rapidly, with $t_{\rm burn}/t_{\rm edd} \simeq 10^9$. At this point, the nuclear burning develops supersonically, and a detonation is initiated.

**We next explore the onset of ignition in more depth. To examine this issue of the spatial resolution of our ignition region, we employ the complementary cumulative distribution function (CCDF). The CCDF is defined to be the cumulative probability down to a specified value; that is, CCDF $(T) = \int_T^\infty {\rm PDF}(T')dT'$. As a result, the CCDF highlights the upper tail of the distribution, which of key relevance to the onset of ignition. In particular, the number of grid cells above a temperature cut $T_{\rm cut}$ is simply given by CCDF $(T_{\rm cut})$ times the total number of grid cells in the computation.**

**In figure 6, we plot the log of the CCDF of the temperature distribution over a number of timesteps subsequent to the onset of detonation for our $512^3$ model. Here we define the onset of detonation to be the time, $t_{\rm det}$ at which the peak temperature reaches $1.9\times10^9$ K, corresponding to the development of a runaway tail of the peak temperature. A cut is placed in the temperature distribution at $T_{\rm cut} = 1.9\times10^9$ K, delineating the ignited material from the remainder of the flow. In the inset, we plot the number of grid cells versus the number of timesteps subsequent to the onset of the detonation. The number of cells rises from zero to approximately 400 by the time the hot spot has developed into a detonation approximately $t_{\rm det} = 0.35$ ms, 52 timesteps later. These results quantitatively demonstrate the hot spot is well-resolved spatially at the onset of detonation.**

**The onset of detonation is further examined in spherically-averaged radial profiles in figure 8. The profiles are taken about a single point of maximum nuclear energy generation at the onset of detonation $t_{\rm det}$, as defined as in figure 6, when the peak temperature in the detonating hot spot reaches $1.9\times10^9$ K. We note that the entire hot spot, and the subsequent detonation,**

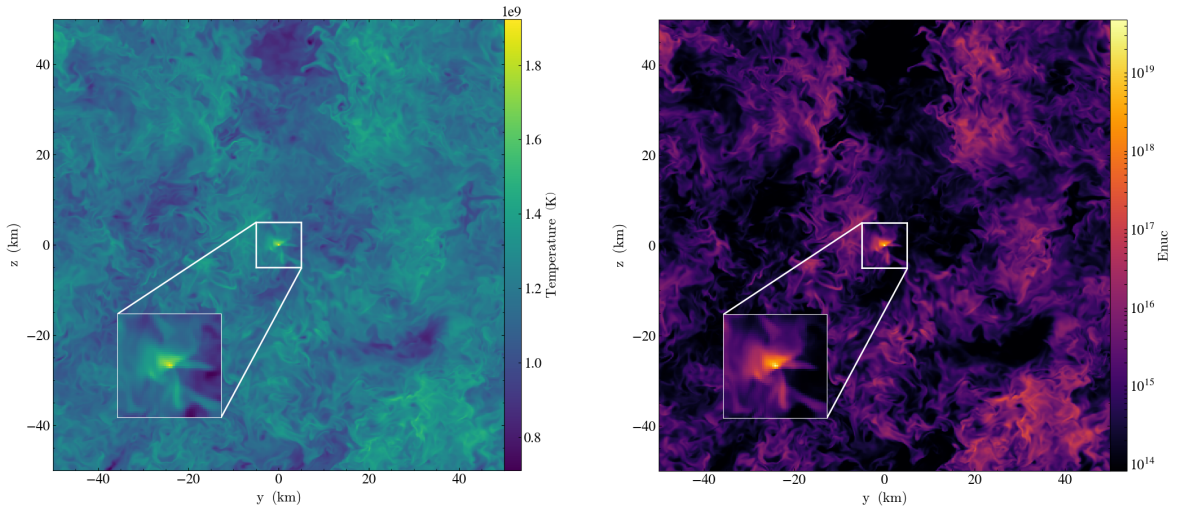


**Figure 3**: Slice plots of temperature and specific nuclear energy generation rate in the $y$-$z$ plane for the $512^3$ run. The point of maximum temperature is centered in the middle of these slices. The slices are taken at $t = 14$ ms, just prior to the onset of detonation for the $512^3$ run. The insets show zooms around the point of maximum temperature and nuclear energy burning, which subsequently develops into a detonation.

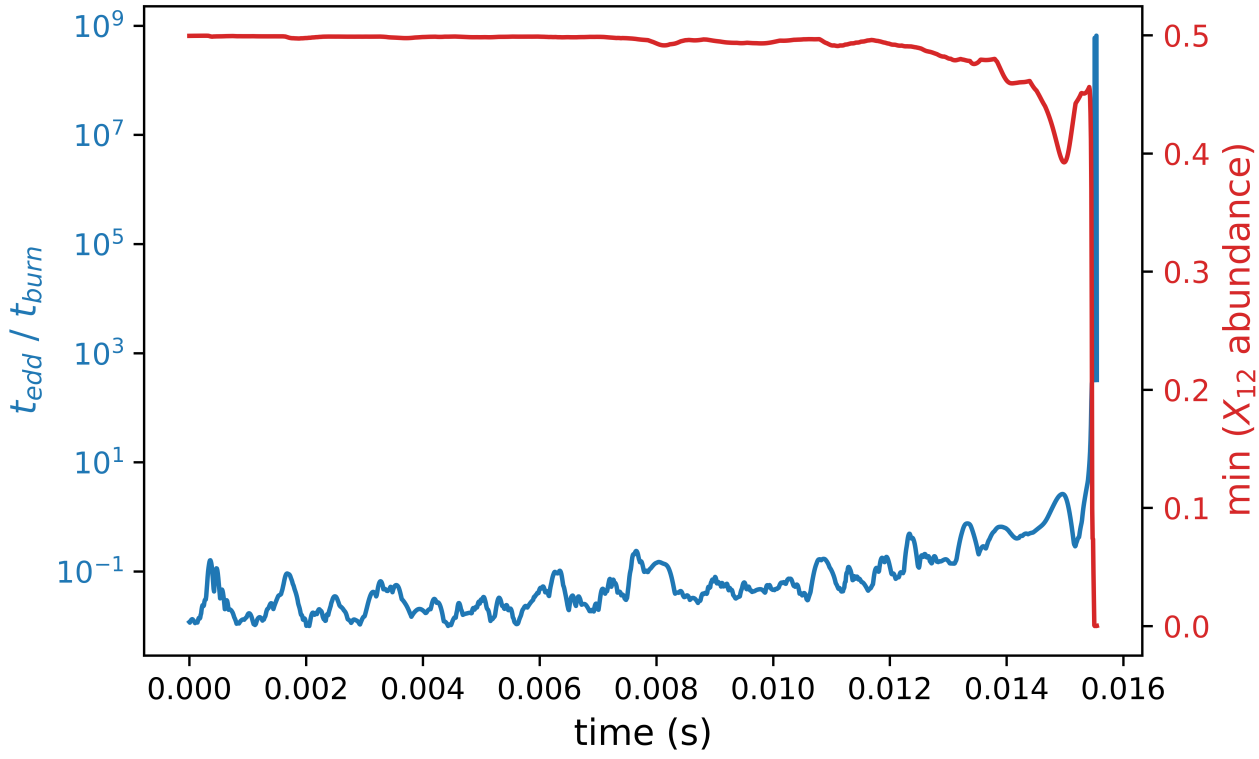


**Figure 4**: Plot of the ratio of the eddy-turnover timescale versus the carbon nuclear burning timescale (left axis, in blue), and the minimum $^{12}$C abundance (right axis, in red) versus simulation time. Local hotspots develop stable nuclear burning before turbulently mixing into the background on a $t_{\rm edd} \simeq 1$ ms timescale. At $t = 0.015$ s, a detonation develops centered at the hot spot of figure 3.

is being advected with the turbulent background flow. However, because the turbulent velocity on the scale of this plot is about an order of magnitude less than the detonation speed, advection has a minimal effect on the radial profiles. Each curve represents 40 timesteps in the simulation, so this time series commences near the end of the CCDF series of figure 6, and extends further in time.

Figure 8 demonstrates the initial hot spot extends over a region of approximately 1 km, or approximately 500 cells, as determined by the full width at half maximum of the temperature profile above the background. This independently confirms the hot spot is spatially well-resolved at $t_{\rm det}$. When the center of the spot exceeds $\sim 2\times10^9$ K, the specific nuclear energy generation exceeds $10^{19}$ erg s$^{-1}$ g$^{-1}$, an enhancement of over three orders of magnitude of the background just a few kilometers away. At this point, the temperature undergoes a runaway, and rapidly grows to a radially-averaged value of $\sim 3.5\times10^9$ K. By $t_{\rm det} = 0.29$ ms, the temperature and the nuclear energy generation rate steepen, and a well-defined detonation front has developed, with temperature and nuclear burning both rising above the background together at the same radial location. The detonation front propagates supersonically at $v_{\rm det} \sim 10^4$ km/s. The width of the profile, particularly as seen in the nuclear energy generation rate profile, extends over 1 - 4 km, and continues to broaden in time. This broadening originates from the spherical averaging of the intrinsically asymmetric propagation of the detonation into the non-uniform turbulent background.

We note that in all simulations presented here, the detonation front which develops propagates successfully until all carbon and oxygen fuel is completely consumed, approximately $L/(2v_{\rm det}) = 5$ ms later. This final successful detonation spot is preceded by a number of hot spots which quench prior to successful detonation, as figure 4 shows. Further, in some models, more than one detonation is initiated within the computational volume in the $\sim 5$ ms needed to completely consume the fuel. The propensity of the simulations to produce multiple hot spots within this short amount of time, amounting to just a few timesteps of fully global 3D simulations of merging white dwarfs, suggests that the turbulently-driven detonation mechanism is sufficiently robust to produce detonations at even lower turbulence levels than presented here.

Previous work on 3D simulations of SNe Ia has emphasized the importance of temporally resolving thermonuclear burning (Hawley et al. 2012; Kashyap et al. 2015). The temporal resolution criterion may be characterized by the maximum fractional change $C_{\rm burn}$ of internal energy imposed per timestep, $\Delta t_{\rm burn} \leq \min(C_{\rm burn} e_{\rm int}/\epsilon_{\rm nuc})$. However, because the spatial resolution in these local simulations is orders of magnitude finer than global SNe Ia simulations, the CFL timestep alone implies a stringent burning timestep. In particular, our $512^3$ model has $C_{\rm burn} \simeq 0.1$ near the onset of detonation. Inspection of the CCDF in figure 6 reveals that the enhancement of the peak temperature from $\sim 2\times10^9$ K to $\sim 4.5\times10^9$ K occurs over the span of approximately 50 timesteps in the $512^3$ model. Consequently, the ignition is well-resolved temporally as well as spatially. In comparison, the most stringent burning timestep achieved in global 3D SNe Ia simulations is $C_{\rm burn} = 0.2 - 0.3$ (Hawley et al. 2012; Kashyap et al. 2015). Convergence tests conducted by imposing an even smaller $C_{\rm burn}$ with one-half the value implied by the CFL did not produce any substantive differences from the models presented here. Additionally, a recent paper (Katz & Zingale 2019) argues that spatial resolutions of 1 km or less are required to achieve convergence during the initiation of detonation. Katz & Zingale use a simplified 1D setup to capture the basic physics of a direct detonation initiation of colliding WDs, which is a considerably different context than the turbulently-driven spontaneous detonation initiation considered in this paper. However, their findings are consistent with our conclusion that our detonation initiations, at spatial resolutions down to 0.2 km, is of physical, and not numerical origin.

## 6. DISCUSSION

There exists a body of work exploring detonation initiation in the distributed burning regime (Lisewski et al. 2000a,b; Woosley 2007; Aspden et al. 2008; Woosley et al. 2009; Aspden et al. 2010; Schmidt et al. 2010; Woosley et al. 2011; Ciaraldi-Schoolmann et al. 2013). Principally, this work was motivated by understanding the properties of burning in near-$M_{\rm Ch}$ WDs in the single-degenerate channel as the flame transitioned from the turbulent flamelet regime into the distributed burning regime.

In this paper, we have built upon and extended this earlier work, being motivated by recent observational and theoretical developments in the dynamics and the burning in WD mergers. In this regards, our work differs primarily from earlier authors in considering turbulence several or-

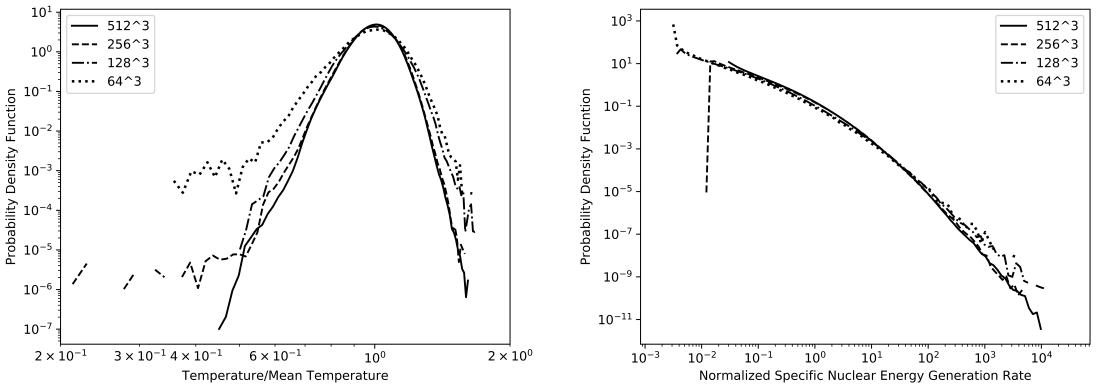


**Figure 5**: The PDFs for the temperature and the specific nuclear burning rate, for each of the four runs, $64^3$, $128^3$, $256^3$, and $512^3$. Each PDF is shown at an equivalent maximum temperature of $2 \times 10^9$ K, just prior to the onset of detonation for each model. In both plots, the PDF is normalized to the mean value of each model.

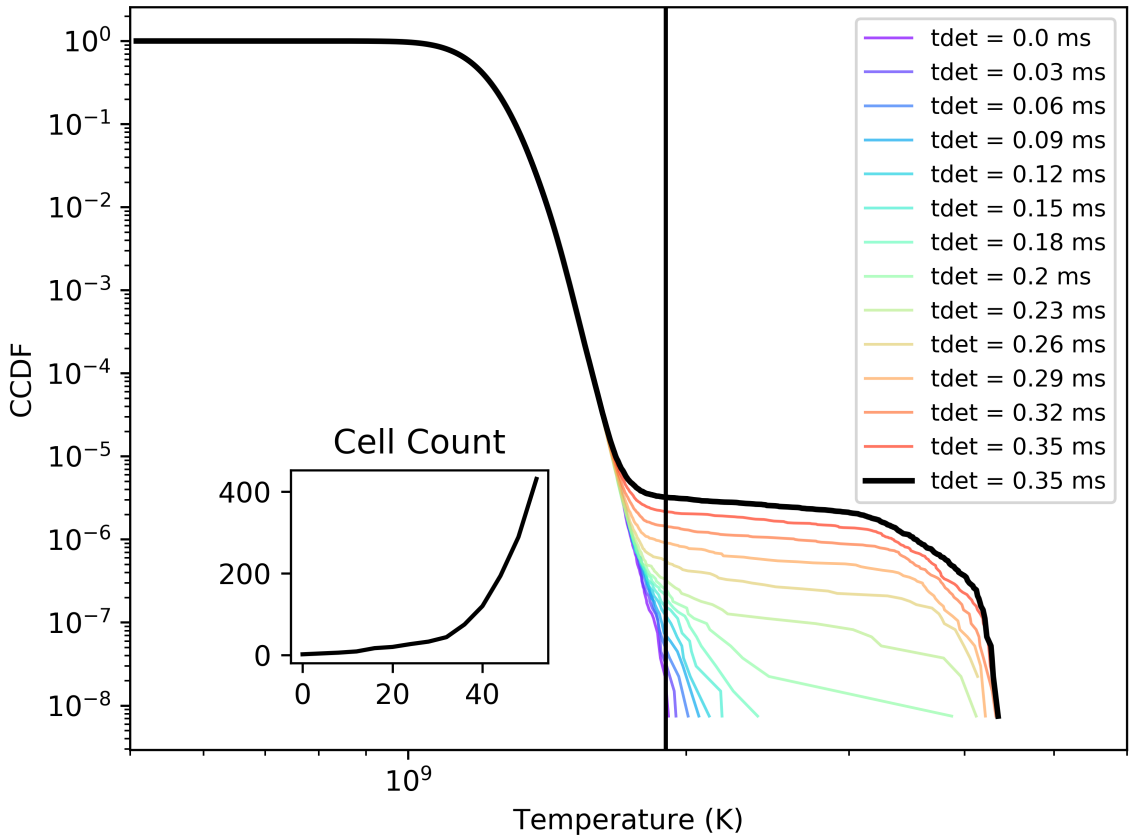


**Figure 6**: A time series of the complementary cumulative distribution function (CCDF), defined in the text, for our $512^3$ simulation. The series begins at the onset of detonation initiation. Each curve corresponds to four timesteps within the simulation. The inset shows the number of grid cells above a temperature cut of $T_{\rm cut} = 1.9 \times 10^9$ K, versus the number of timesteps subsequent to the onset of ignition. The inset demonstrates that the detonation initiation is resolved both temporally and spatially, with approximately 50 timesteps and 400 grid cells, respectively.

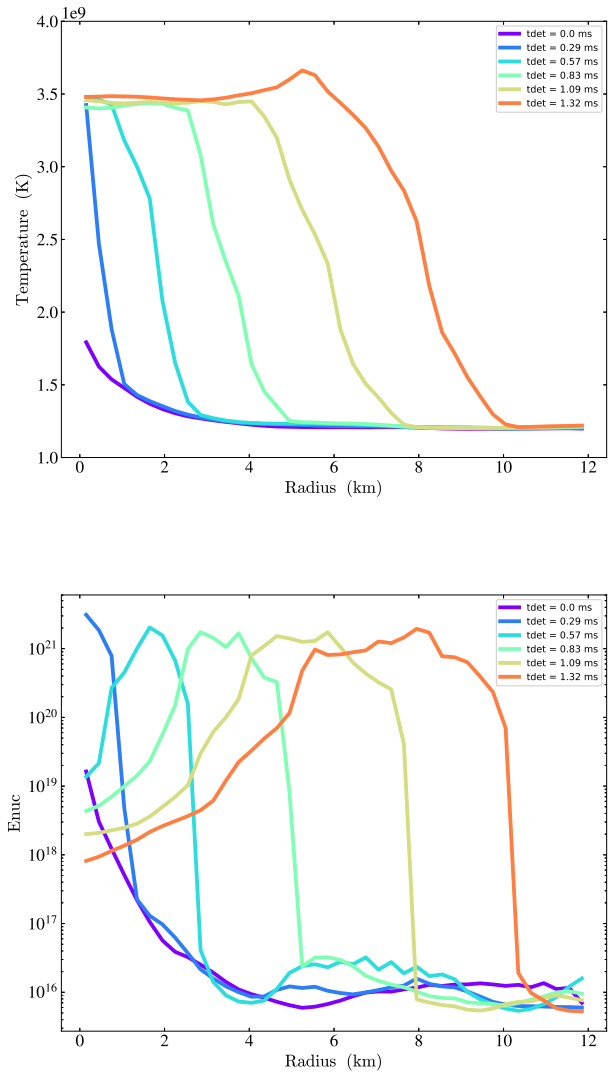


**Figure 8**: Spherically-averaged radial profiles of both the temperature and the specific nuclear burning rate for the $512^3$ model at the onset of detonation, as described in the text.

**ders of magnitude larger than previously considered. The mean turbulent dissipation $v^3/L \sim 10^{18}$ erg g$^{-1}$ s$^{-1}$ considered here is typical of shear-driven turbulence in WD mergers, which approach the orbital velocity at merger, or roughly $\sim$ few $\times 10^3$ km/s. However, this level of turbulence was typically considered implausible in near-$M_{\rm Ch}$ WDs, where the emerging flame bubble typically has a buoyant velocity which is limited by drag to $\sim$ 100 km/s. For example, the *highest* mean dissipation considered in fully-three dimensional simulations of turbulent distributed flame by Aspden et al. (2010) is of the order of $10^{15}$ erg g$^{-1}$ s$^{-1}$, three orders of magnitude smaller than the mean dissipation considered here. None of the computational models considered by Aspden and colleagues led to a detonation.**

**As a direct consequence of the lower levels of turbulence typically considered in the previous literature, it is challenging to naturally explain the origin of a possible deflagration-to-detonation transition in near-$M_{\rm Ch}$ WDs in the distributed burning regime. For example, Lisewski et al. (2000a) and Lisewski et al. (2000b) concluded, based upon one-dimensional turbulence modeling, that Karlovitz numbers of order $10^4$ were required to initiate a detonation in the distributed burning regime. They further estimated that Rayleigh-Taylor driven turbulence in flame bubbles in the near-$M_{\rm Ch}$ WDs implied Ka $\sim 10$ – three orders of magnitude smaller than their estimated requirement. Lisewski et al concluded that the level of turbulence expected was too low to initiate detonation in the distributed burning regime. However, the Karlovitz number for the simulations presented here is $7\times10^3$, close to Lisewski et al's original estimated value for detonation initiation in the distributed burning regime. Our findings therefore suggest that the basic frameworks developed in theoretical models of near-$M_{\rm Ch}$ WDs may be fruitfully applied to and verified against computational models of the much stronger turbulence expected in merging white dwarfs.**

## 7. CONCLUSION

Previous physically-motivated detonations in the carbon-oxygen WD core in 3D double degenerate WD simulations, e.g. (Pakmor et al. 2010; Kashyap et al. 2015), have adopted criteria based upon the combined density and temperature within a given cell or smoothed particle hydrodynamics (SPH) particle to infer whether a detonation is likely according to the Zel'dovich gradient mechanism. The resulting simulations are typically too slowly-declining (Pakmor et al. 2010), with too great a viewing angle dependence (Moll et al. 2014), too much polarization (Bulla et al. 2016), and predict too few events (Liu et al. 2018), in comparison to normal SNe Ia. This disagreement between simulations and observations poses questions about the viability of the double-degenerate channel as a primary explosion channel for the majority of SNe Ia, and has motivated the introduction of alternative models, such as colliding WDs (Kushnir et al. 2013).

However, the imposition of the Zel'dovich gradient mechanism in global SNe Ia simulations neglects the

important role of turbulence on detonation initiation. Turbulently-driven detonation initiation within the distributed burning regime naturally leads to a wider range of mean density and temperature conditions than previously realized. This broader range of predicted detonation initiation conditions has ramifications for leading SNe Ia channels, in which the onset of the detonation is predicted to arise under highly dynamical and turbulent conditions.

**Acknowledgements** RTF gratefully acknowledges conversations with Enrique García-Berro, a close collaborator who tragically passed away in 2017, which inspired this work. RTF also thanks the Institute for Theory and Computation at the Harvard-Smithsonian Center for Astrophysics for visiting support during which a portion of this work was undertaken. RTF acknowledges support from NASA **80NSSC18K1013**. This work used the Extreme Science and Engineering Discovery Environment (XSEDE) Stampede 2 supercomputer at the University of Texas at Austin's Texas Advanced Computing Center through allocation TG-AST100038, supported by National Science Foundation grant number ACI-1548562 (Towns et al. 2014).

*Software:* We utilize the adaptive mesh refinement code FLASH 4.0.1, developed by the DOE NNSA-ASC OASCR Flash Center at the University of Chicago. For plotting and analysis, we have made use of yt (Turk et al. 2011), http://yt-project.org/.

## REFERENCES


Arnèodo, A., Benzi, R., Berg, J., et al. 2008, Physical Review Letters, 100, 254504, doi: 10.1103/PhysRevLett.100.254504

Arnett, D., & Livne, E. 1994, ApJ, 427, 330, doi: 10.1086/174143

Aspden, A. J., Bell, J. B., Day, M. S., Woosley, S. E., & Zingale, M. 2008, ApJ, 689, 1173, doi: 10.1086/592726

Aspden, A. J., Bell, J. B., & Woosley, S. E. 2010, ApJ, 710, 1654, doi: 10.1088/0004-637X/710/2/1654

Benzi, R., Biferale, L., Fisher, R., Lamb, D. Q., & Toschi, F. 2010, Journal of Fluid Mechanics, 653, 221, doi: 10.1017/S002211201000056X

Benzi, R., Biferale, L., Fisher, R. T., et al. 2008, Physical Review Letters, 100, 234503, doi: 10.1103/PhysRevLett.100.234503

Benzi, R., Ciliberto, S., Tripiccione, R., et al. 1993, Phys. Rev. E, 48, R29, doi: 10.1103/PhysRevE.48.R29

Blinnikov, S. I., & Khokhlov, A. M. 1986, Soviet Astronomy Letters, 12, 131

—. 1987, Soviet Astronomy Letters, 13, 364

Bulla, M., Sim, S. A., Pakmor, R., et al. 2016, MNRAS, 455, 1060, doi: 10.1093/mnras/stv2402

Churazov, E., Sunyaev, R., Isern, J., et al. 2014, Nature, 512, 406, doi: 10.1038/nature13672

Ciaraldi-Schoolmann, F., Seitenzahl, I. R., & Röpke, F. K. 2013, A&A, 559, A117, doi: 10.1051/0004-6361/201321480

Dan, M., Rosswog, S., Brüggen, M., & Podsiadlowski, P. 2014, MNRAS, 438, 14, doi: 10.1093/mnras/stt1766

Dubrulle, B. 1994, Phys. Rev. Lett., 73, 959, doi: 10.1103/PhysRevLett.73.959

Federrath, C., Roman-Duval, J., Klessen, R. S., Schmidt, W., & Mac Low, M.-M. 2010, A&A, 512, A81, doi: 10.1051/0004-6361/200912437

Fenn, D., & Plewa, T. 2017, MNRAS, 468, 1361, doi: 10.1093/mnras/stx524

Fisher, R. T., Kadanoff, L. P., Lamb, D. Q., et al. 2008, IBM Journal of Research and Development, 52, 127, doi: 10.1147/rd.521.0127

Frisch, U. 1995, Turbulence: The Legacy of A. N. Kolmogorov (Cambridge University Press), doi: 10.1017/CBO9781139170666

Garcia-Senz, D., & Woosley, S. E. 1995, ApJ, 454, 895, doi: 10.1086/176542

Gotoh, T., Fukayama, D., & Nakano, T. 2002, Physics of Fluids, 14, 1065, doi: 10.1063/1.1448296

Guillochon, J., Dan, M., Ramirez-Ruiz, E., & Rosswog, S. 2010, ApJL, 709, L64, doi: 10.1088/2041-8205/709/1/L64

Hawley, W. P., Athanassiadou, T., & Timmes, F. X. 2012, ApJ, 759, 39, doi: 10.1088/0004-637X/759/1/39

Holcomb, C., Guillochon, J., De Colle, F., & Ramirez-Ruiz, E. 2013, ApJ, 771, 14, doi: 10.1088/0004-637X/771/1/14

Jayesh, & Warhaft, Z. 1991, Physical Review Letters, 67, 3503, doi: 10.1103/PhysRevLett.67.3503

Kashyap, R., Fisher, R., García-Berro, E., et al. 2015, ApJL, 800, L7, doi: 10.1088/2041-8205/800/1/L7

Katz, M. P., & Zingale, M. 2019, arXiv e-prints. https://arxiv.org/abs/1903.00132

Khokhlov, A. M., Oran, E. S., & Wheeler, J. C. 1997, ApJ, 478, 678, doi: 10.1086/303815

Kolmogorov, A. N. 1962, Journal of Fluid Mechanics, 13, 82–85, doi: 10.1017/S0022112062000518

Kushnir, D., Katz, B., Dong, S., Livne, E., & Fernández, R. 2013, ApJL, 778, L37, doi: 10.1088/2041-8205/778/2/L37

Lisewski, A. M., Hillebrandt, W., & Woosley, S. E. 2000a, ApJ, 538, 831, doi: 10.1086/309158

Lisewski, A. M., Hillebrandt, W., Woosley, S. E., Niemeyer, J. C., & Kerstein, A. R. 2000b, ApJ, 537, 405, doi: 10.1086/309015

Liu, D., Wang, B., & Han, Z. 2018, MNRAS, 473, 5352, doi: 10.1093/mnras/stx2756

Moll, R., Raskin, C., Kasen, D., & Woosley, S. E. 2014, ApJ, 785, 105, doi: 10.1088/0004-637X/785/2/105

Nandkumar, R., & Pethick, C. J. 1984, MNRAS, 209, 511, doi: 10.1093/mnras/209.3.511

Niemeyer, J. C. 1999, ApJL, 523, L57, doi: 10.1086/312253

Niemeyer, J. C., & Woosley, S. E. 1997, ApJ, 475, 740, doi: 10.1086/303544

Nugent, P. E., Sullivan, M., Cenko, S. B., et al. 2011, Nature, 480, 344, doi: 10.1038/nature10644

Oboukhov, A. M. 1962, Journal of Fluid Mechanics, 13, 77–81, doi: 10.1017/S0022112062000506

Pakmor, R., Kromer, M., Röpke, F. K., et al. 2010, Nature, 463, 61, doi: 10.1038/nature08642

Pakmor, R., Kromer, M., Taubenberger, S., & Springel, V. 2013, ApJL, 770, L8, doi: 10.1088/2041-8205/770/1/L8

Phillips, M. M. 1993, ApJL, 413, L105, doi: 10.1086/186970

Poinsot, T., & Veynante, D. 2005, Theoretical and Numerical Combustion (Edwards). https://books.google.com/books?id=cqFDkeVABYoC

Poludnenko, A. Y. 2015, Physics of Fluids, 27, 014106, doi: 10.1063/1.4905298

Poludnenko, A. Y., Gardiner, T. A., & Oran, E. S. 2011, Physical Review Letters, 107, 054501, doi: 10.1103/PhysRevLett.107.054501

Pope, S. B. 2000, Turbulent Flows (Cambridge University Press), doi: 10.1017/CBO9780511840531
Röpke, F. K., Woosley, S. E., & Hillebrandt, W. 2007, ApJ, 660, 1344, doi: 10.1086/512769
Saw, E.-W., Debue, P., Kuzzay, D., Daviaud, F., & Dubrulle, B. 2018, Journal of Fluid Mechanics, 837, 657, doi: 10.1017/jfm.2017.848
Schmidt, W., Ciaraldi-Schoolmann, F., Niemeyer, J. C., Röpke, F. K., & Hillebrandt, W. 2010, ApJ, 710, 1683, doi: 10.1088/0004-637X/710/2/1683
Schmidt, W., Niemeyer, J. C., & Hillebrandt, W. 2006, A&A, 450, 265, doi: 10.1051/0004-6361:20053617
Seitenzahl, I. R., Meakin, C. A., Townsley, D. M., Lamb, D. Q., & Truran, J. W. 2009, ApJ, 696, 515, doi: 10.1088/0004-637X/696/1/515
She, Z.-S., & Leveque, E. 1994, Phys. Rev. Lett., 72, 336, doi: 10.1103/PhysRevLett.72.336
Sreenivasan, K. R. 1995, Physics of Fluids, 7, 2778, doi: 10.1063/1.868656
Timmes, F. X. 1999, ApJS, 124, 241, doi: 10.1086/313257
Timmes, F. X., & Swesty, F. D. 2000, The Astrophysical Journal Supplement Series, 126, 501–516, doi: 10.1086/313304
Timmes, F. X., & Woosley, S. E. 1992, ApJ, 396, 649, doi: 10.1086/171746
Towns, J., Cockerill, T., Dahan, M., et al. 2014, Computing in Science Engineering, 16, 62, doi: 10.1109/MCSE.2014.80
Turk, M. J., Smith, B. D., Oishi, J. S., et al. 2011, ApJS, 192, 9
Weaver, T. A., Zimmerman, G. B., & Woosley, S. E. 1978, ApJ, 225, 1021, doi: 10.1086/156569
Woosley, S. E. 2007, ApJ, 668, 1109, doi: 10.1086/520835
Woosley, S. E., Kerstein, A. R., & Aspden, A. J. 2011, ApJ, 734, 37, doi: 10.1088/0004-637X/734/1/37
Woosley, S. E., Kerstein, A. R., Sankaran, V., Aspden, A. J., & Röpke, F. K. 2009, ApJ, 704, 255, doi: 10.1088/0004-637X/704/1/255
Zel'dovich, Y. B., Librovich, V. B., Makhviladze, G. M., & Sivashinskil, G. I. 1970, Journal of Applied Mechanics and Technical Physics, 11, 264, doi: 10.1007/BF00908106